




Small-scale diagenetic facies heterogeneity controls porosity and permeability pattern in reservoir sandstones

Matthias Heidsiek¹ · Christoph Butscher² · Philipp Blum³ · Cornelius Fischer^{1,4} 

Received: 14 February 2020 / Accepted: 3 September 2020 / Published online: 15 September 2020
© The Author(s) 2020

Abstract

The fluvial-aeolian Upper Rotliegend sandstones from the Bebertal outcrop (Flechtingen High, Germany) are the famous reservoir analog for the deeply buried Upper Rotliegend gas reservoirs of the Southern Permian Basin. While most diagenetic and reservoir quality investigations are conducted on a meter scale, there is an emerging consensus that significant reservoir heterogeneity is inherited from diagenetic complexity at smaller scales. In this study, we utilize information about diagenetic products and processes at the pore- and plug-scale and analyze their impact on the heterogeneity of porosity, permeability, and cement patterns. Eodiagenetic poikilitic calcite cements, illite/iron oxide grain coatings, and the amount of infiltrated clay are responsible for mm- to cm-scale reservoir heterogeneities in the Parchim formation of the Upper Rotliegend sandstones. Using the Petrel E&P software platform, spatial fluctuations and spatial variations of permeability, porosity, and calcite cements are modeled and compared, offering opportunities for predicting small-scale reservoir rock properties based on diagenetic constraints.

Keywords Sandstone diagenesis · Calcite cement · Reservoir quality · High-resolution diagenetic modeling · Upper Rotliegend sandstone

Introduction

Understanding diagenetic processes and their effect on porosity and permeability distribution and heterogeneity has been an important research topic for several decades (e.g., Bjørlykke and Jahren 2012). This research was, and is, largely driven by the petroleum industry, but it is also important for the evaluation of alternative energy solutions, such as geothermal reservoirs and gas storage. Failure to recognize diagenetic effects on porosity and permeability can lead to large errors in reservoir volume estimation and can influence production strategies and rates (e.g., Ajdukiewicz and Lander 2010). The last decades of research have added significantly to the understanding of how diagenesis affects reservoir quality and heterogeneity, but predicting reservoir quality of deeply buried sandstones remains a major challenge (Taylor et al. 2010). As of now, there is no general framework for modeling or predicting diagenetic cement distribution patterns in sandstones. However, such an approach would be very useful for predicting the heterogeneity of porosity or permeability of a primary sedimentary unit.

The depositional porosity of a rock is rarely retained and is generally degraded by various diagenetic processes,

This article is a part of the Topical Collection in Environmental Earth Sciences on “Sustainable Utilization of Geosystems” guest edited by Ulf Hünken, Peter Dietrich and Olaf Kolditz.

Electronic supplementary material The online version of this article (<https://doi.org/10.1007/s12665-020-09168-z>) contains supplementary material, which is available to authorized users.

✉ Cornelius Fischer
c.fischer@hzdr.de

- ¹ University of Bremen, FB Geowissenschaften, Klagenfurter Str., 28359 Bremen, Germany
- ² TU Bergakademie Freiberg, Institute of Geotechnics, Gustav-Zeuner-Str. 1, 09599 Freiberg, Germany
- ³ KIT, Institute of Applied Geosciences (AGW), Kaiserstraße 12, 76131 Karlsruhe, Germany
- ⁴ Helmholtz-Zentrum Dresden-Rossendorf (HZDR), Institut für Ressourcenökologie, Abt. Reaktiver Transport, Permoserstr. 15, 04318 Leipzig, Germany

unrestricted spatially to the boundaries of the sedimentary units (e.g., Worden and Matray 1998). The diagenetic evolution of sandstones often results in a superimposition of multiple types of newly formed diagenetic minerals. The heterogeneous spatial distribution of such cements is responsible for a complex porosity and permeability pattern at the pore scale and above. Therefore, predicting the distribution of porosity and permeability of deeply buried sandstones and understanding their diagenetic control is crucial for reservoir applications (Taylor et al. 2010).

The distribution of diagenetic alterations and reservoir heterogeneity at the scale of tens-of-meters to kilometers is related to sediment composition, depositional facies, and sequence stratigraphy of sandstones (Morad et al. 2010). However, predicting reservoir heterogeneity, the distribution of diagenetic alterations, and their controlling factors within each depositional facies and sandstone unit remains a major challenge (Worden et al. 2018). This is particularly true for more complex systems that are affected by eodiagenetic features, such as grain coatings, carbonate cements, and mesodiagenetic features such as secondary porosity. Usually, such features are included in current reservoir models through observations and analogs rather than a priori predictions (e.g., Ajdukiewicz and Lander 2010; Morad et al. 2010; Taylor et al. 2010). This highlights the incomplete understanding of the controlling factors of reservoir heterogeneity and the need to further investigate reservoir rocks to identify the key processes

that drive plug-scale reservoir quality and heterogeneity in different geological settings (Taylor et al. 2010). Usually, the spatial resolution of 3D grids used for porosity and facies modeling is at the meter scale. As an example, Kimple et al. (2015) report a cell size of 20 ft × 20 ft × 1 ft forming a 3D grid of 300 rows by 300 columns and 200 layers. This example illustrates the spatial detail of porosity and facies heterogeneity of an oilfield. In our example, we use a similar number of cells. However, our focus is on the analysis of spatial heterogeneity and predictability of permeability vs. intergranular volume and porosity, on the plug scale as suggested in previous studies (e.g., Taylor et al. 2010), thus using a cell size in the mm range.

In this study, we focus on identification and improved understanding of small-scale spatial heterogeneity of calcite cement patterns in reservoir sandstones. The Petrel E&P software platform is used to develop a high-resolution 3D model of fluvial-aeolian sedimentary facies with a grid size capable of modeling cement patterns on the centimeter scale. Usually, larger trends of diagenetic contrasts are tied to the distribution of sedimentary facies bodies and to the burial history (e.g., Worden et al. 2018). Our main research question is: Can a high-resolution model of cement patterns predict the fluctuations of permeability and porosity in a reservoir? Using high-resolution permeability, porosity, and calcite cement data, we test the ability of correlating reservoir quality and cement concentration patterns on the centimeter scale (Fig. 1). In addition, we provide a workflow of

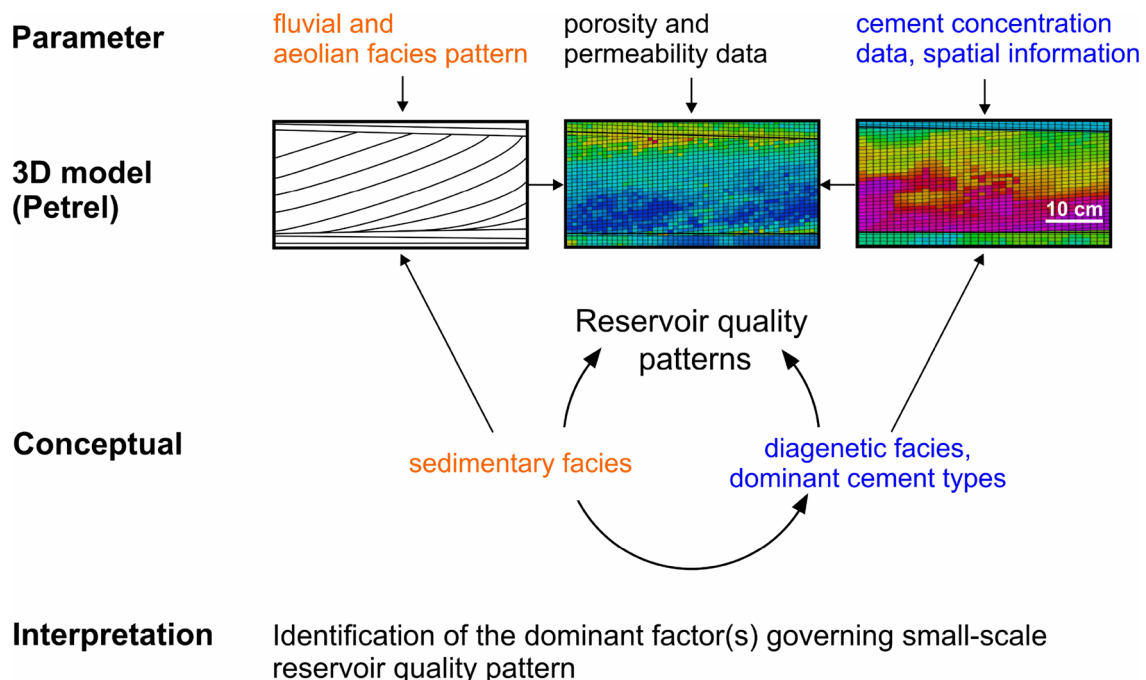


Fig. 1 Conceptual approach of utilizing a high-resolution model focusing on the identification of small-scale diagenetic facies patterns that can explain spatial heterogeneity of porosity and permeability

how to use petrographic data to create high-resolution 3D rock-property models.

Materials and methods

Geological setting

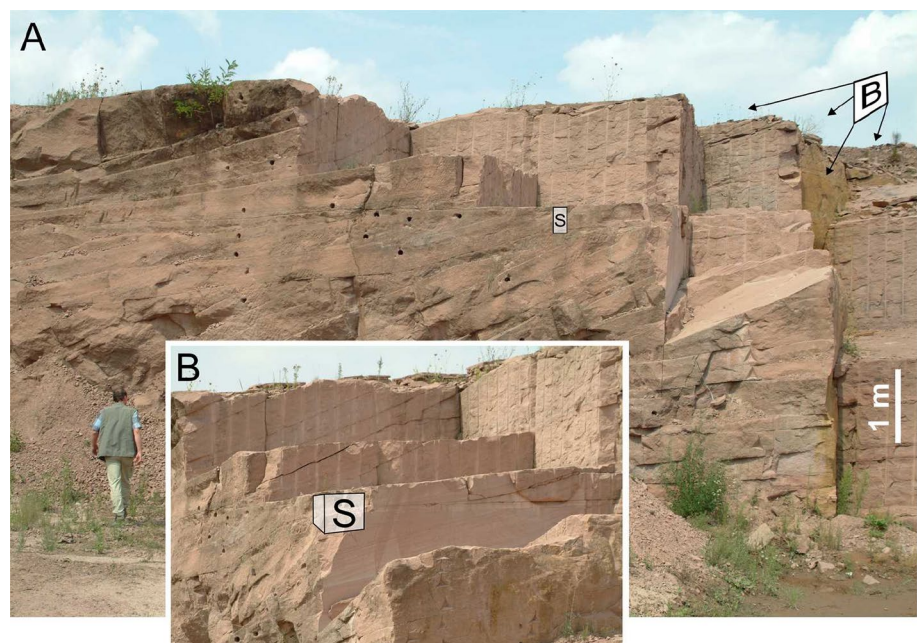
We investigated sandstones from the Bebertal quarry, located 28 km NW of Magdeburg (cf. GK25 map 3733: Erxleben, R 44 52 700/H 57 89 800) (Ellenberg et al. 1976; Fischer et al. 2007, 2012) (Fig. 2).

The Bebertal outcrop offers insight into the Upper-Rotliegend fluvial-aeolian sandstone facies of the Flechtingen Bausandstein (Fig. 2) and belongs to the Parchim Formation (Havel sub-group) of the South Permian Basin (SPB) (Kleditzsch and Kurze 1993; Plein 1993). This outcrop has been an active quarry until recently, thus a large amount of information on the three-dimensional sedimentary facies distribution has been collected during the last decades, until about 10 years ago (Dolbert 1998; Ellenberg et al. 1976; Fischer 2013; Schreiber 1960). The upper 12 m of the outcropping section (Fig. 2) consist of laminated and cross-bedded aeolian sandstones with thin layers of fluvial sheet-flow deposits consisting of clay-rich sands, gravels, and cross-bedded fluvial sands. This predominately aeolian section overlies about 20 m of fluvial sandstones and conglomerates. Detailed information about the sedimentary facies is available from several drill cores (Fischer et al. 2007). The Bebertal outcrop is of particular interest because it is the northern-most outcrop of the Upper Rotliegend sandstones in Central Europe. In addition, it is

the only one that contains time-equivalent sandstones of similar sedimentary facies properties as those that form the prolific gas reservoirs of the North German Basin (NGB) as part of the SPB (Fig. 3). Today, these reservoirs are located 3000–6000 m below the surface across north Germany, the Netherlands, and Poland (Gaupp and Okkerman 2011; Grötsch and Gaupp 2011; Grötsch et al. 2011; Kulke et al. 1993; Poszytek 2013; Schöner and Gaupp 2005; Wong et al. 2007).

The Parchim Formation was deposited on the southern flanks of the NGB during the Guadalupium of the Permian. The formation is predominantly composed of lithic subarcosic aeolian dune sandstones and poorly sorted fluvial sandstones and conglomerates. To the south, the formation changes into an alluvial fan and wadi deposits and the formation interfingers with lacustrine deposits of a vast salt lake towards the main basin depocenter (Conford 1998; Gast et al. 2010; Kulke et al. 1993). After deposition ~266 Ma ago, the fluvial-aeolian sands of the Parchim Formation were quickly buried and reached their maximum burial during Early to Middle Triassic (Fischer et al. 2012). During the Late Cretaceous-Early Cenozoic inversion, the Flechtingen High block was rapidly uplifted by 3–4 km in only a few million years (Fischer et al. 2012; Gemmer et al. 2003; Glennie 1986). Due to the tectonic history, the sandstones of the Parchim Formation were heavily altered by diagenetic reactions and products, making this formation a very suitable candidate to study the influence of diagenetic products on reservoir heterogeneity over a wide range of length scales, i.e., from the micrometer to centimeter scale.

Fig. 2 Fluvial-aeolian sandstones outcropping in the Bebertal quarry. Aeolian cross-bedded sandstones intercalate with sub-horizontally bedded fluvial and aeolian strata. Signature “S” indicates the approximate position of the sample block (length = 45 cm) investigated in this study. The view of (a) is in north-eastern direction, the detailed view of (b) is in north-western direction



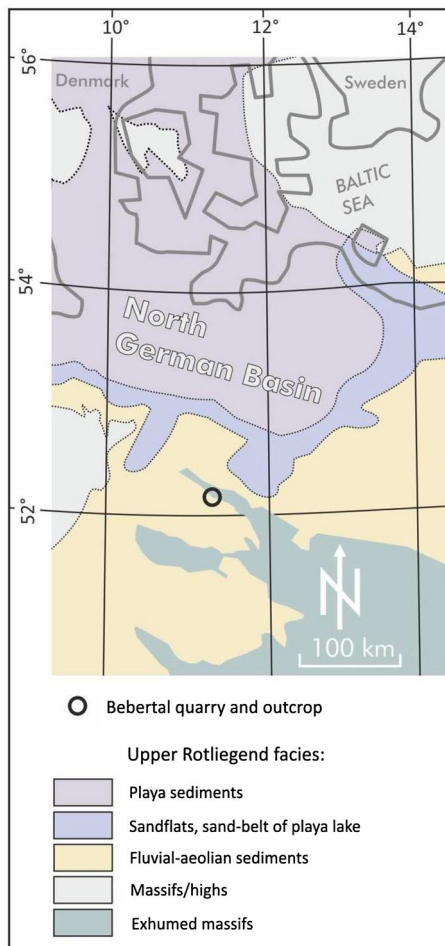


Fig. 3 Paleo-depositional map of the North German Basin, part of the Southern Permian Basin. The circle symbol (o) marks the approximate location of the Bebertal outcrop (Flechtingen High) within the fluvial-aeolian facies (Upper Rotliegend), deposited along the edges of the basin. This outcrop is the main reservoir analog for the North German gas fields focusing on small-scale sedimentary facies and bounding surface geometry, modified after Gast et al. (2010)

Sample material

The sample selected for this study is a medium- to fine-grained lithic subarcosic fluvial-aeolian sandstone. The size of the sample block is 39 cm × 45 cm × 11.5 cm. The sandstone sample contains four main sedimentary bounding surfaces separating the sample into five sedimentary layers (Fig. 4). The top and bottom layer are fluvial sheet-flow deposits. The three sedimentary layers in between the fluvial sheet flows are cross-bedded/laminated, medium-to-fine-grained, lithic, subarcosic, aeolian sandstone (Fischer et al. 2007).

The fluvial sheet-flow deposits represent seasonal/occasional deposition events related to heavy rainfall in an otherwise arid desert environment, which resulted in debris flows that deposited poorly sorted clay-rich sands, gravels,

and clean sands as fan/sheet-like sediment bodies (e.g., Fryberger 1993; Mountney et al. 1998; Mountney and Jagger 2004).

The cross-bedded aeolian sandstones were formed by dune migration, depositing sand through grain avalanches on the lee side of the dune. This resulted in homogenous and well-sorted 0.5–3 cm thick laminations/dune foresets that are separated by thin pinstripes. The laminated aeolian sandstone was deposited by the migration of sand ripples. This created thin, sheet-like lamination with a thickness of 0.2–1.5 cm that are also separated by pinstripes. The sorting of this layer is not as good as the cross-bedded sandstone (well to moderate) and the grain size ranges from very-fine to coarse sand (Fryberger 1993; Fryberger and Schenk 1988; Jones et al. 2016; Kulke et al. 1993; Scherer and Lavina 2005).

Methods

Qualitative and quantitative analyses of rock properties were conducted to characterize and document with high spatial resolution the sedimentary facies and diagenetic minerals, as well as the porosity and permeability properties of the Upper Rotliegend sandstones. Figure 5 illustrates the sample grid utilized for several methods.

Permeability measurements

The permeability measurements were used as input for the reservoir quality model and as a guide for selecting the subsequent locations for the thin section samples, so as to represent contrasting permeability properties (Fig. 5). The measurements were taken using the syringe air permeameter TinyPerm 3, developed and manufactured by New England Research Inc. (NER). The instrument is a portable handheld air permeameter designed to measure permeability in the range of 1 millidarcy (mD) to 10 darcys (D) on outcrop and core samples (Brown and Smith 2013). The ability of the instrument to measure the permeability of porous rock and fractures was shown in several studies (e.g., De Boever et al. 2016; Filomena et al. 2014; Hale et al. 2019). It was also successfully used to evaluate aquifer heterogeneity and spatial variation of hydraulic aquifer properties (e.g., Huysmans et al. 2008; Rogiers et al. 2014a) and to relate permeability variation to diagenetic processes (e.g., Fischer et al. 2013; Gaupp 1996; Molenaar et al. 2015). According to previous investigations (e.g., Molz III et al. 2003; Rogiers et al. 2014b), the investigation depth of the air permeameter (with 8 mm inner diameter of the tip) in the present study is suggested to be in the order of about 1 cm resulting in a sampled volume of about 2 cm³. A total of 303 measurement points were placed on both sides of the rock sample (Fig. 5). Each measurement point was measured at least 3 times for

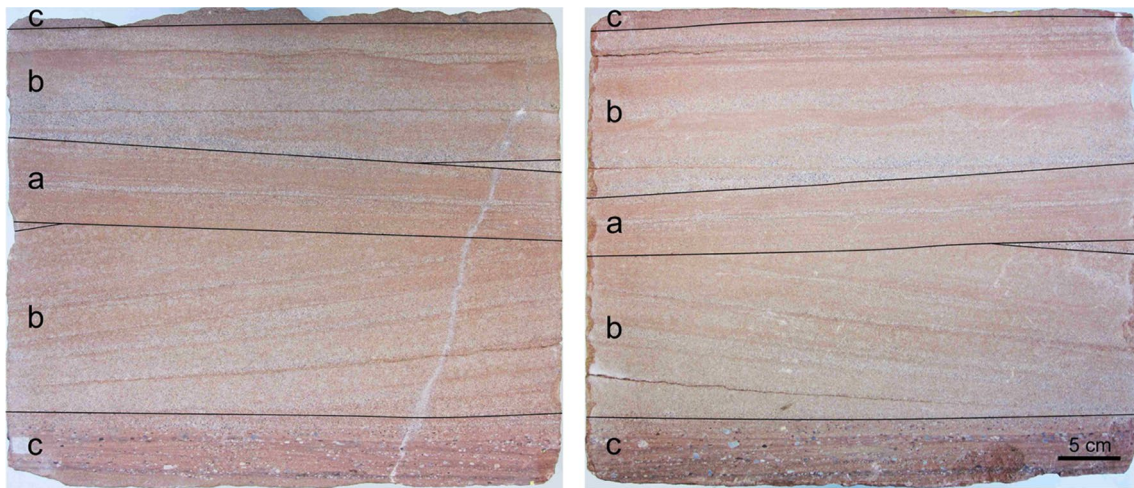


Fig. 4 Sample block of mostly medium-to-fine-grained, lithic, subarcotic fluvial-aeolian sandstones. Sample size is 39 cm×45 cm×11.5 cm. Black lines indicate sedimentary bounding

surfaces separating the sample into 5 distinct facies layers consisting of (a) laminated and (b) cross-bedded aeolian deposits in-between c poorly sorted fluvial sheet-flow deposits

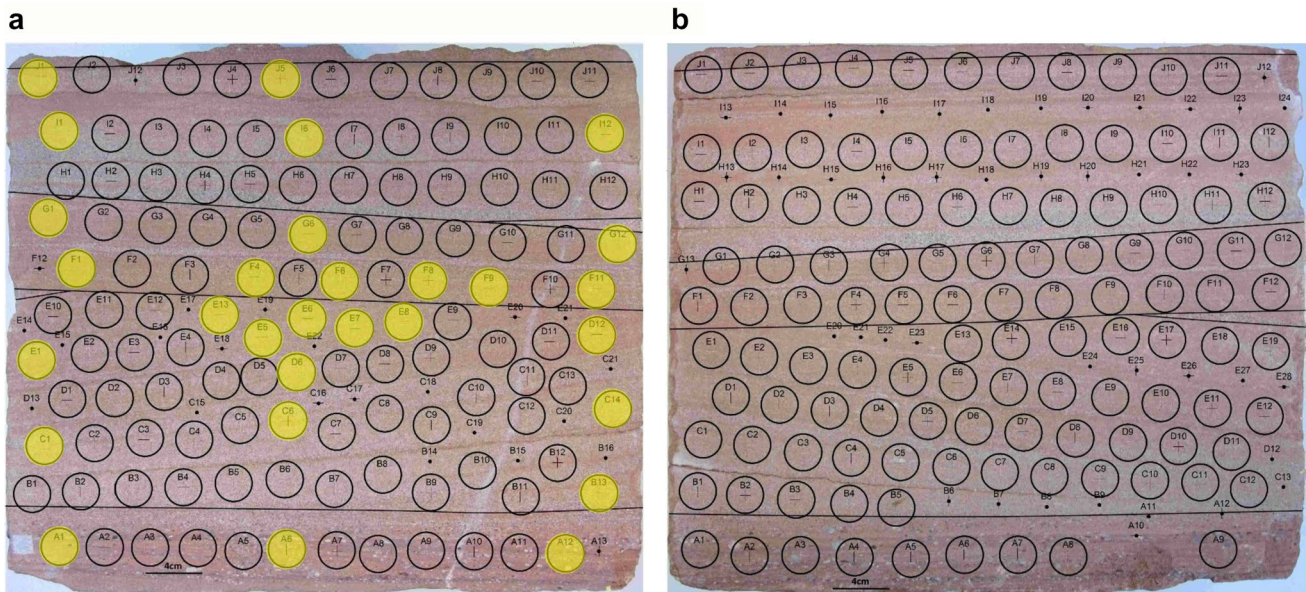


Fig. 5 Front (a) and back (b) side of the sample block with locations of 303 permeability measurement points. The 29 sample points marked in yellow were selected for additional petrographic analysis. Samples were selected to cover the range of lithological composition,

permeability (mD) and depositional facies. Each sample is identified by a sample ID. The letter identifies the facies type (Fig. 4) and the number identifies the sample within a single facies unit

30–60 s per measurement, depending on local permeability. After the completion of all measurements, the mean permeability, standard deviation, and standard error were calculated for each sample point. For all further analysis, the mean permeability of each point was used. Throughout the measurement process, the TinyPerm 3 performed very well, averaging a standard deviation of 0.86 mD and an average standard error (SE) of 0.46 mD for the repeated measurements. These numbers show that the instrument displays a

high level of precision even in a low-permeability environment in which most of the samples are close to the advertised detection limit of 1 mD.

Thin-section petrography and image analysis

29 thin-section samples were analyzed to identify the diagenetic history and compare the observations with previous investigations about the paragenetic sequence (Fischer et al.

2012). The thin-sections were taken from the end of about 6 cm long core plugs drilled at each corresponding permeability measurement point. Thus, due to the high heterogeneity of the sample block, some thin-sections do not represent the same rock properties as the surface location used for the permeability measurements, cf. Fig. SI 3. The calcite cement volume and porosity were quantified for each sample by picture segmentation based on color thresholding. The scan under normal light was used for the thresholding of the

porosity. The picture provides a sharp contrast between the blue-dyed epoxy resin and the mineral grains. The scan collected under crossed polarizers was used for the quantification of the calcite cement using the high-interference colors of the calcite mineral, which creates a good contrast to the greys of the mineral grains. The segmentation results for each sample were visually quality-controlled, and wrongly identified pores or cements were manually removed or corrected. The results from the quantitative image analysis were used as an input into the final model and to create porosity and calcite cement distribution maps for each sample (cf. Fig. 6).

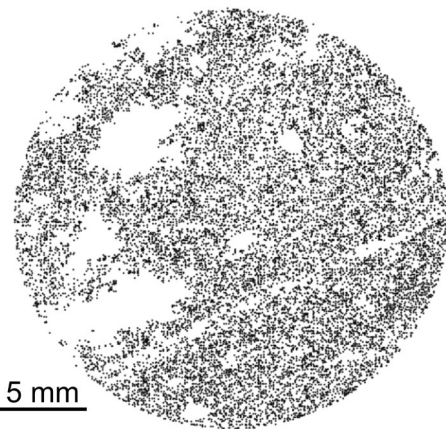


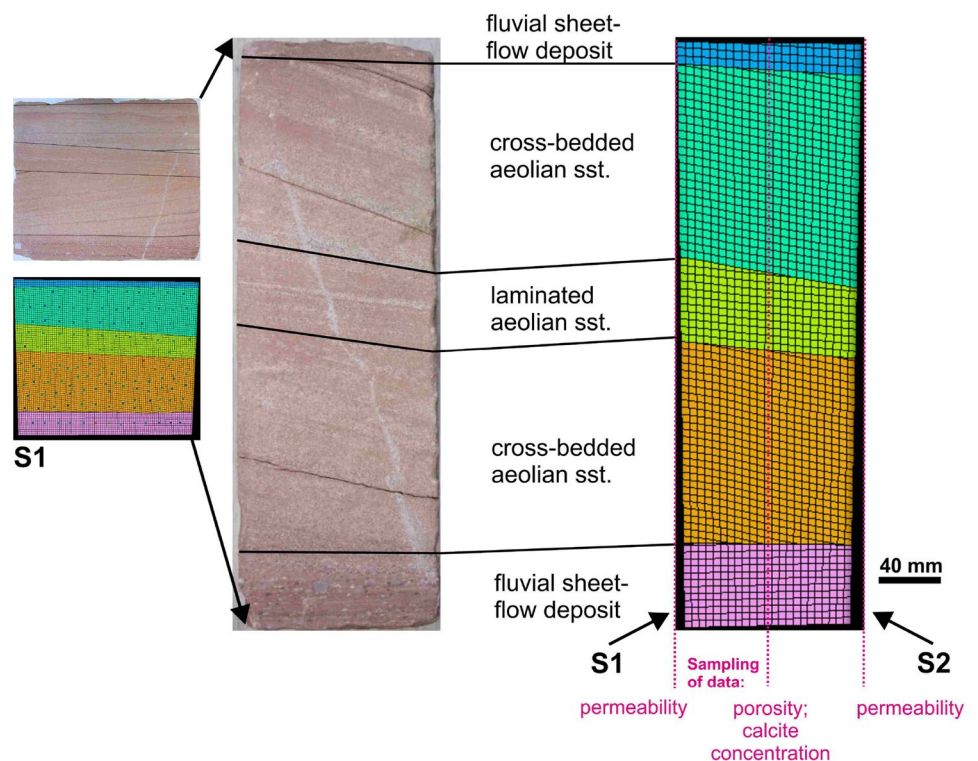
Fig. 6 Example of segmented porosity distribution, thin section sample E13. The porosity was plotted using the *X* and *Y* coordinates of each segmented pore from the image analysis. The blank areas are zones that do not show any porosity

Modeling

Petrel 2017 (Schlumberger) was used to create the 3D model of the sample block. The simulation grid, i.e., the 3D replication of the sample block, creates the boundary conditions for the porosity, permeability, and cementation model, based on the sedimentary facies (Fig. 4). The simulation grid has a cell size of 5 mm × 5 mm × 5 mm and is separated into the five main sedimentary units by four horizons. The layering within each section is arranged in such a way that it is mimicking the dip of the strata and the lamination. The entire simulation grid is composed of 194,580 3D cells (Fig. 7).

After defining the simulation grid, the permeability, porosity, and calcite cement data points were integrated into the model. The permeability data points were placed on the

Fig. 7 Simulation grid provides the boundary conditions for the model, size is 39 cm × 45 cm × 11.5 cm. The simulation grid has a cell size of 5 mm × 5 mm × 5 mm and is separated into the five main sedimentary units, as observed in the sample, left side. Positions of permeability, porosity, and calcite cement concentration data are indicated



surfaces S1 and S2 of the model volume (Fig. 7). The data points for the porosity and the calcite cement were placed in the middle of the model grid because the thin sections were retrieved from the end of the 5–6 cm long core plugs. The reservoir modeling was performed using the Sequential Gaussian Simulation (SGS) method which can reproduce the heterogeneity observed in the input data.

The calcite cement is the most voluminous cement in the formation and one of the main contributors to reservoir heterogeneity. Thus, the model approach requires a method that is capable of reproducing the heterogeneity observed in the input data. For that reason, the Sequential Gaussian Simulation (SGS) method was chosen as the modeling algorithm to model the reservoir quality throughout the sample block. The SGS process consists of the following steps (Pyrzcz and Deutsch, 2014): (a) transformation of the original input data to a standard normal distribution, (b) placing the transformed data into the modeling grid, (c) going to a random grid node u and searching for neighboring data and previously modeled data values, (d) performing kriging with those values to obtain kriged estimate and corresponding kriging variance, (e) drawing a random residual that follows a normal distribution with mean = 0 and the local variance at grid node u ; the residual is drawn with a classical Monte Carlo simulation, (f) adding the simulated data to the data set so it will be used for the simulation of the next simulated value, (g) visiting all grid nodes in the simulation grid in a random order, and (h) back-transforming all data values and simulated values after the model is fully populated. All these steps are performed automatically by the software except for the data transformation (a) and the variogram analysis, which is part of the kriging process (d) within the SGS algorithm.

The parameters for these processes were set separately for each model section and each data set. The SGS method also allows for the creation of any number of realizations by repeating the process and starting with a different random number seed. A different seed leads to a different random path and different residuals for each simulated grid node. Each realization is equally likely to be drawn and, therefore, called equiprobable, allowing to evaluate the uncertainty of the model. After each simulation, the model output must be checked to make sure it honors the input data. The first step is a visual inspection to check if the model behaved as expected, focusing on high- and low-value areas and trends. The second step is to check the data reproduction. This process includes comparing input data parameters like mean, standard deviation, variance, and variogram to the model output to see how well they were reproduced (Pyrzcz and Deutsch 2014).

The data transformation process included several steps as illustrated in Fig. 8. First, the output truncation was applied to ensure that the final model did not contain any

data outside of the input range. The second step was to detect any strong vertical trends and extract them from the data (Fig. 8b, c), as they can heavily influence the variogram and mask the smaller trends in the variance of the data. The third and fourth steps were to apply the shift-scale transformation to generate a distribution with a mean = 0 and standard deviation = 1 (Fig. 8d) and to apply the normal score transformation to force the distribution into a standard normal distribution (Fig. 8e). This is necessary since the SGS takes place in the Gaussian space. After modeling, the data were back-transformed to their original state and the extracted trends were added back in. These steps were applied to the sedimentary facies volumes. For the permeability data of the upper cross-bedded aeolian section, the standard normal score transformation could not be applied because of the extreme bimodal distribution of the data. The measurements range from 0.26 to 3.56 mD, with an average of 1.49 mD, with the exception of five measurement points (S2: H17–H21), which range from 10.86 to 140.26 mD and are clustered in one area. This creates a data set with a mean, standard deviation, and variance not representative of the entire cross-bedded section. Oversampling areas with abnormally high values that only represent a small portion of the overall formation is quite common in geological evaluations, since those areas are normally of high interest (e.g. high gold concentrations, high permeability). The software offers a solution, allowing for the fitting of the distribution to the input data, creating a more representative probability curve, rather than trying to span a bell curve over the entire data range. This approach allowed for the modeling of the permeability values for the upper cross-bedded section to be based on the actual occurrence from the input data, thereby creating a more realistic model. Consequently, the mean, standard deviation, and variance from the input data will not be reproduced and, therefore, cannot be used to evaluate the fit of the model for that section.

For the variogram analysis of the data, a spherical regression curve was chosen as the best fit for the data. A search cone defines which samples are included in the variogram analysis (Pyrzcz and Deutsch 2014). During the variogram analysis for the SGS, three variograms for three different directions were created. The major direction was defined as cutting the block horizontally, parallel to the 45 cm long edge. The minor range was defined as cutting the block horizontally, parallel to the 11.5 cm long edge. The third variogram was for the vertical direction. The analysis of the spatial distribution of the variance in all three directions allows for the capture of the heterogeneity of the formation in all three directions. During modeling, the SGS algorithm uses the major, minor, and vertical ranges as well as the sill and nugget from the variogram model to reproduce the heterogeneity of the input data. This creates a more realistic distribution of values throughout the modeled rock volume.

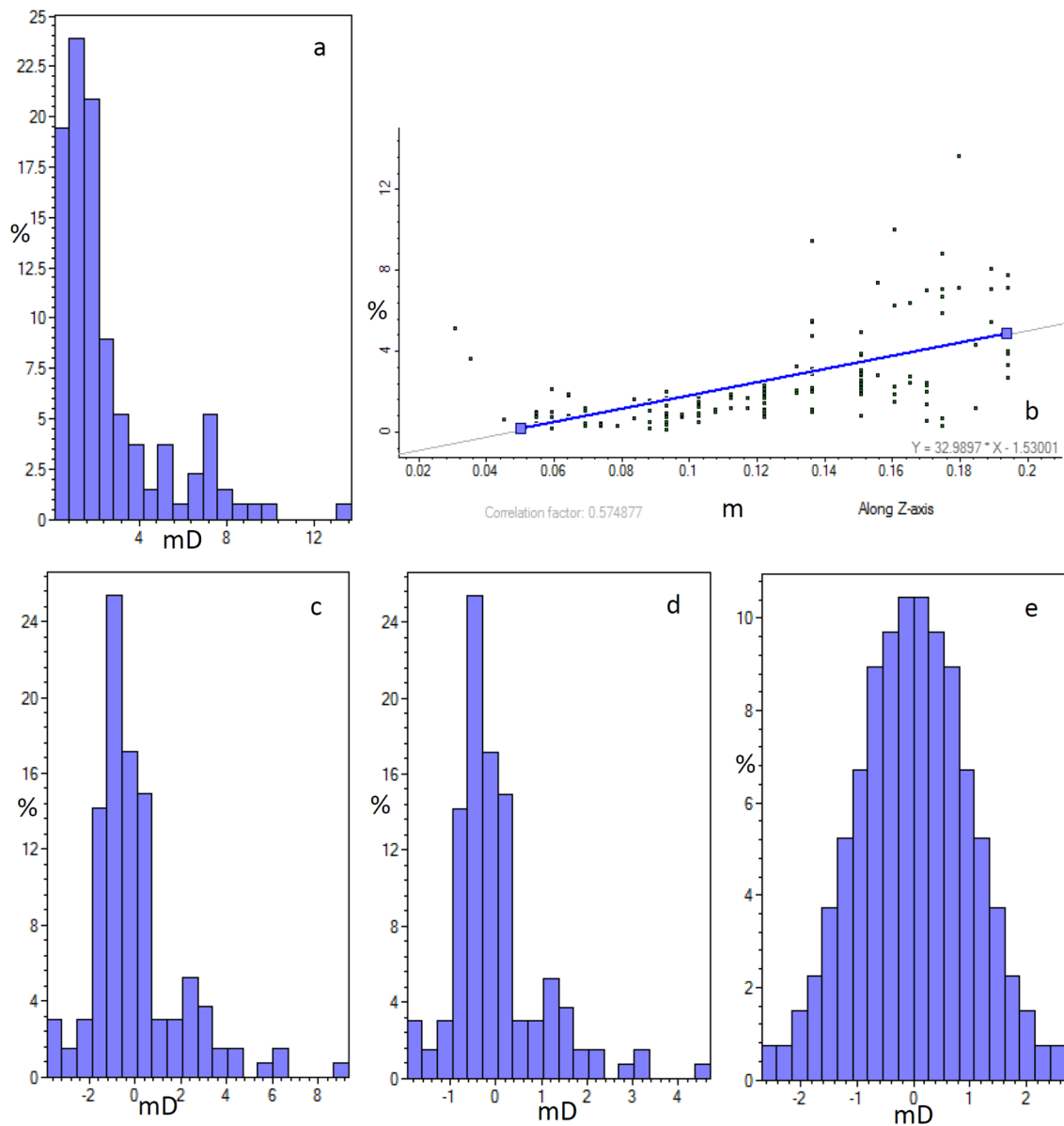


Fig. 8 Example of the data transformation performed on a set of permeability data before starting SGS modeling, details include **a** input data, **b** detection and extraction of vertical trends, **c** data after the

removal of the vertical trend, **d** data after the shift scale transformation, and **e** data after the normal score transformation

Since the porosity and calcite cement volume data are based on only 29 sample points, the data density is much lower than the 303 data points for permeability. This led to complications in creating the variograms. The upper cross-bedded sandstone and the fluvial section only contain five and three sample points, respectively. Because of this, only a vertical variogram could be constructed for the calcite and porosity data in the upper cross-bedded sandstone. The variogram settings for the major and minor directions were based on the variogram analysis of the permeability data. In the fluvial section, none of the three variograms could be constructed

for the calcite and porosity data due to the low sample density. Therefore, the variogram settings from the permeability data were used. Adapting the variogram settings from the permeability data was done as a best approximation of the expected variance of the calcite cement and porosity data in the sample.

Each sedimentary package was modeled separately to prevent the mixing of data from different sedimentary layers, which can obscure small-scale heterogeneity trends. The top layer was not modeled as it was too thin to be sampled. During the modeling process, porosity, permeability, and

calcite cement were modeled independently without using the empirical relationships between the parameters as a model input.

Results and discussion

Eodiagenetic and mesodiagenetic poikilitic calcite cements, mesodiagenetic illite/iron oxide grain coatings, and the amount of infiltrated clay are the main causes of cm-scale (plug-scale) reservoir heterogeneities in the Parchim Formation of the Upper Rotliegend sandstones. They were identified via thin-section petrography investigations. Detailed previous investigations on the diagenetic history of these strata revealed eodiagenetic poikilitic and late-mesodiagenetic calcite formation, cf. the paragenetic sequence including age determinations of K-feldspar cements (Fischer et al. 2012). A new interpretation is the existence of additional early-mesodiagenetic poikilitic calcite in the material sampled for this study. In addition to early-diagenetic poikilitic calcite, this second calcite generation precipitated after the formation of the first diagenetic potassium feldspar generation but before the previously reported younger mesodiagenetic cements.

Data about calcite cement concentration, porosity, and permeability are loaded into a model, details are provided in the SI section. The spatial heterogeneity of this data is analyzed using a detailed variogram analysis, see chapter 2.3.3. Compared to a multitude of other simulation studies (e.g., Jones et al. 2009), we used this software for modeling a rather small rock volume (39 cm × 45 cm × 11.5 cm) to test the capabilities of interpreting and predicting the small-scale fluctuations and spatial heterogeneity of permeability, porosity, and cement volume distribution.

Petrographic results and diagenetic history

Three vertical profiles of the sample block were analyzed via thin-section petrography, details are reported in the SI section. Quantitative petrographic data included porosity volume, total calcite cement volume, poikilitic calcite (early diagenetic + early mesodiagenetic), and late mesodiagenetic calcite. Thin-section analysis revealed five distinct diagenetic facies types (Fig. 9):

- (F1) High porosity/permeability facies,
- (F2) Calcite cement facies,
- (F3) Low IGV (intergranular volume) facies (occurring in both fluvial and aeolian deposits),
- (F4) Fluvial high porosity facies, and
- (F5) Fluvial claystone facies.

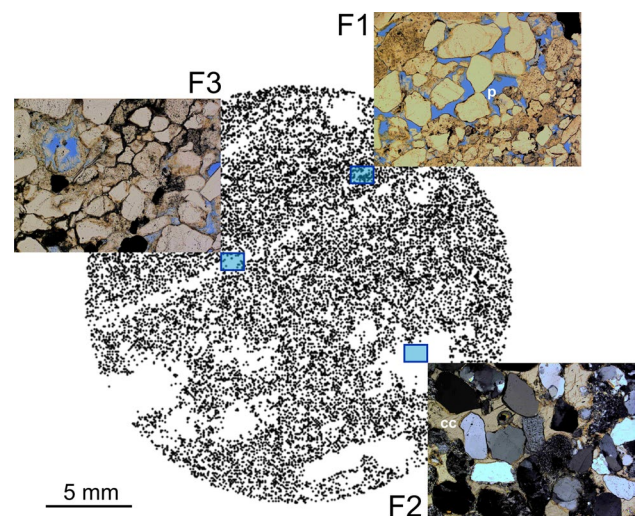


Fig. 9 Three endmembers of the porosity and diagenetic properties typical for the cross-bedded aeolian sandstone (sample E8, cf. Figure 5), illustrating the heterogeneity of porosity distribution at the plug scale. The mm-scale heterogeneity is dictated by the different diagenetic facies F1–3 (F1: high intergranular volume and low cement concentration, F2: high intergranular volume and early-diagenetic poikilitic calcite cements, F3: pinstripes aeolian facies with low intergranular volume). Note the occurrence of secondary porosity owing to K-feldspar dissolution (F3) (*p* pores, *cc* calcite cement)

These facies do not occur in large patches that dominate an entire sedimentary unit (Fig. 4). Instead, different facies types occur together in close proximity within aeolian (F1–3) or fluvial (F4, 5) units, creating the cm-scale heterogeneity observed in the rock volume. An example of the aeolian units is shown in Fig. 9, sample E8 (Fig. 5a).

Permeability, porosity, and calcite cement pattern and heterogeneity

The permeability ranges from 0.12 to 140.26 mD with most sample points (287) ranging from 1 to 10 mD, only 8 sample points above 10 mD, and 90 sample points exhibiting permeabilities below 1 mD. The laminated aeolian deposit (f–g; cf. Fig. 5) is the largest and most homogenous high-permeability area (Table 1) in the sample with permeabilities of up to 12.73 mD. The areas above and below show lower permeabilities, mostly in the range of < 1–2 mD, with a few areas of elevated permeabilities of up to 13.71 mD (Table 1). As an outlier, the upper cross-bedded aeolian section of S2 shows a very localized high-permeability feature (measurement points H17–H21), with permeabilities ranging from 10.86 to 140.26 mD. In no other section of the sample were such high permeabilities measured. However, this layer is only a few millimeters thick and does not extend over the entire width of the sample and was not detected on S1. Overall, the permeability measurements show considerable permeability

Table 1 Average permeabilities κ of the different sedimentary facies (spots A–J; see Fig. 5), measured on the front (S1) and back (S2) side of the sample block

| Sedimentary facies | κ (mD) S1 | κ (mD) S2 |
|--|------------------|--|
| Upper cross-bedded aeolian deposit (H–J) | 1.49 | 1.31 (without spots H17–H21); spots H17–H21: 70.62 |
| Laminated aeolian deposit (F–G) | 4.98 | 3.86 |
| Lower cross-bedded aeolian deposit (B–E) | 2.89 | 2.12 |
| Lower fluvial sheet-flow (A) | 2.47 | 2.00 |

Note the locally enhanced permeability; measured on side S2 of the upper cross-bedded aeolian facies, sample spots H17–21

variations not only in between sedimentary bodies but also inside the sedimentary units themselves, with a permeability decline from S1 to S2 of about 20% over a distance of only 11.5 cm. This is related to the permeability decline towards less-steep cross-bedding. Also notable is the fact that there is not a distinct difference in average permeabilities between the cross-bedded aeolian and the fluvial sediments.

Porosity and permeability of the aeolian sandstones in the Parchim formation are mainly controlled by illite/iron oxide clay grain coatings, the amount of calcite and quartz cement present, and K-feldspar dissolution adding to the overall porosity (Fig. 9, F1–3). The small-scale contrast of the intergranular volume and local differences in compaction efficiency are discussed in the literature (Fischer et al. 2012). The grain coatings inhibit the formation of large amounts of pore-filling quartz cements and K-feldspar cements (Taylor et al. 2010, 2015). The effect of preserving reservoir quality through inhibiting quartz and feldspar cementation is efficient when comparing the lower cross-bedded and laminated aeolian sandstone to the upper cross-bedded aeolian sandstone (Fischer et al. 2012). The upper cross-bedded section, even though it only contains low amounts of calcite cement (0.3–5.4%), shows the lowest average permeability of the entire sample (Fig. 10). The thin section analysis showed that the upper cross-bedded sandstone has less-prevalent grain coatings, and as a result is heavily quartz cemented, including large patches of eogenic poikilitic quartz cement (Fig. 10, micrograph 1a, 1b). This considerably reduces porosity and permeability, leading to the control of reservoir quality in the upper cross-bedded sandstone by the amount of quartz cement. In the lower cross-bedded and in the laminated aeolian sandstone, the grain coatings are much more prevalent, allowing only very limited amounts of quartz and K-feldspar overgrowth cements to develop. Accordingly, throughout those two sections, no poikilitic quartz cement was identified.

The porosity and permeability in the lower cross-bedded sandstone and laminated sandstone are mainly controlled by the amount of calcite cement, which ranges from 2.6 to 19.1% (Fig. 10, micrograph 2a vs. 2b). Of this, around 2/3 of the entire volume is early poikilitic calcite cements. The source for the calcite must have been external, making

fluid-flow throughout the early diagenesis the main factor for when and where calcite cement occurs (Glennie et al. 1978; McBride et al. 1987). The permeability in the fluvial deposit is controlled by the amount of infiltrated iron oxides and clay minerals (Fig. 10, micrographs 3a, 3b). The volume of quartz and feldspar overgrowth cements in the fluvial section is very low due to extensive grain coatings allowing a localized slightly enhanced permeability pattern.

Model of permeability, porosity, and calcite cement concentration

The purpose of this model is to evaluate the opportunities to predict and explain cm-scale heterogeneity with respect to porosity and permeability, and to test the hypothesis of the dominant effect of calcite cementation on the first order variability in reservoir properties. The second goal was to test whether the limited number of porosity and cement concentration data allows for a reliable implementation and explanation of major heterogeneities and trends observed in the high-resolution permeability data of the 3D volume. A sensitivity analysis using three equiprobable realizations for each modeled parameter was performed to gage the reproducibility of the model results. Each realization is associated with a random seed number which allows for the reproduction of the exact result under the same model conditions (“Modeling”). Each realization of every model was able to reproduce the input data parameters such as mean, standard deviation, and variance, giving high confidence in the accuracy of the model and the validity of each realization, see SI section.

Through the entire 3D model, distinct reservoir permeability, porosity, and calcite cement volume trends can be observed. This is expected since they are composed of the same sedimentary bodies, but it also further validates the model as it shows continuity that is supported by the input data (Fig. 11). The permeability model (Fig. 11, upper part) shows characteristic trends within and in-between the analyzed four sandstone sections (b, a, b, c). The effect of both sedimentary bounding surfaces, as well as the aeolian lamination and orientation of the laminae is observed; see the

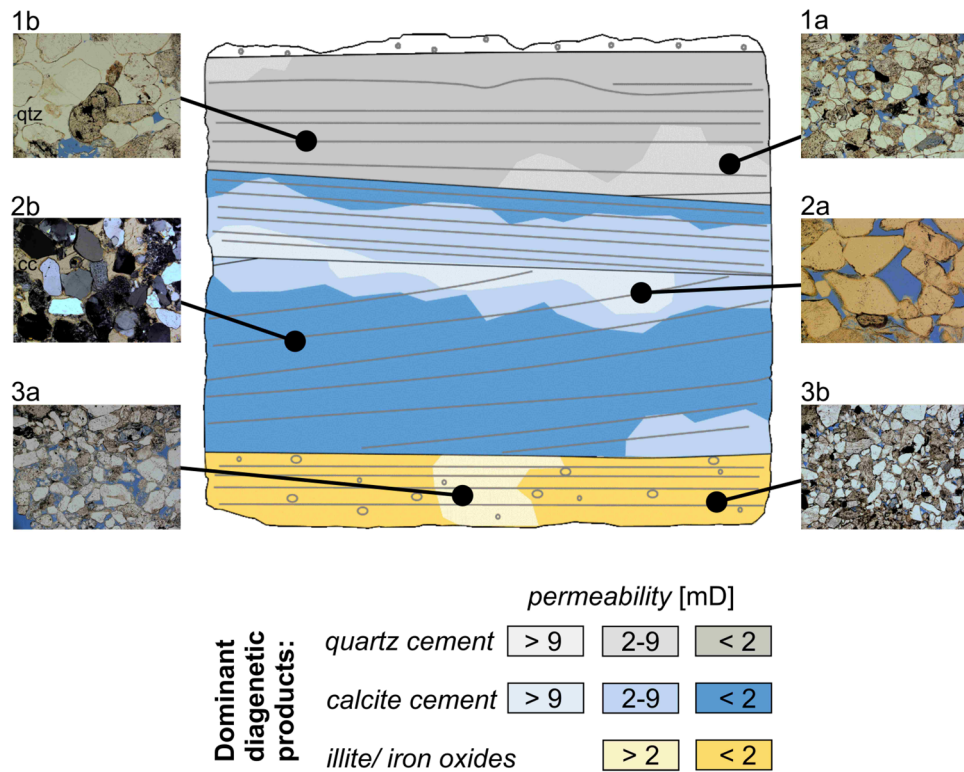


Fig. 10 Schematic sketch of the dominating diagenetic products (i.e., quartz, calcite, and clay/iron oxide) and their relation to permeability patterns of the sample block. First-order cement variability is connected to the sedimentary facies and the occurrence of fluvial-aeolian/inter-aeolian bounding surfaces. The permeability pattern in the lower cross-bedded and laminated aeolian sandstone is controlled by the amount of calcite cement (micrographs 2a, 2b). Areas with the highest amount of permeability/porosity (2a) exhibit calcite cement

values as low as 2.5–4%. The permeability of the upper cross-bedded aeolian sandstone is controlled by the amount of quartz cement (1a, 1b). Here, the illite/iron oxide grain coatings are less prevalent, which allowed more quartz and feldspar cement growth (1b). The permeability in the fluvial deposit reflects the concentration of iron oxides and clay mineral grain coatings (3a, 3b). Image length of the micrographs is = 1.2 mm

two zones of the lower cross-bedded section (b) and laminated aeolian sandstone (a).

The main overall trend that can be recognized in the model is a considerable decline in permeability from S1 to S2. This decline is controlled by the steepness of the aeolian laminations, with the bedding dipping towards S2. The relationship between the steepness of the bedding and the reservoir quality can be especially well-recognized in the lower cross-bedded section. There, the trend of lower permeability and porosity in the areas where the laminations are less-steep is clearly visible. The highest permeability and porosity region is located right below the sedimentary bounding surface, where the bedding is the steepest. The decrease of the reservoir quality between steepest cross-bedding and the less-steep section is significant, ranging from 0.12 to 13.71 mD (permeability) and 1.6–6.9% (porosity). The decrease of permeability between the two sides of the sample block is around 20%. Given the relatively short distance, this is a significant reduction, indicating lateral and vertical reservoir heterogeneity in the formation. This pattern

related to the steepness of the bedding was recognized previously (Fischer et al. 2007, 2012), suggesting that low-angled cross-bedded sandstones have lower intergranular volume due to higher compaction than more steeply cross-bedded sandstone. However, this current investigation shows the opposite, with the less-steep cross-bedding with the lowest reservoir quality being the most heavily cemented, with calcite cement values of up to 19%. This illustrates the impact of diagenetic facies, e.g., quartz- vs. calcite-dominated early diagenetic products and contrasting compaction behavior as well as the need for mapping diagenetic facies types (Gaupp 1996; Gaupp et al. 1993).

In addition to the larger trends, the model also suggests the main controlling mechanism for the reservoir quality when correlating the three models (Fig. 11). This is particularly true for the lower cross-bedded and laminated aeolian sandstones that accurately demonstrate how the permeability and the porosity display the same trends and patterns and how the calcite cement trends are opposite to those trends throughout the entire 3D volume. This shows how porosity

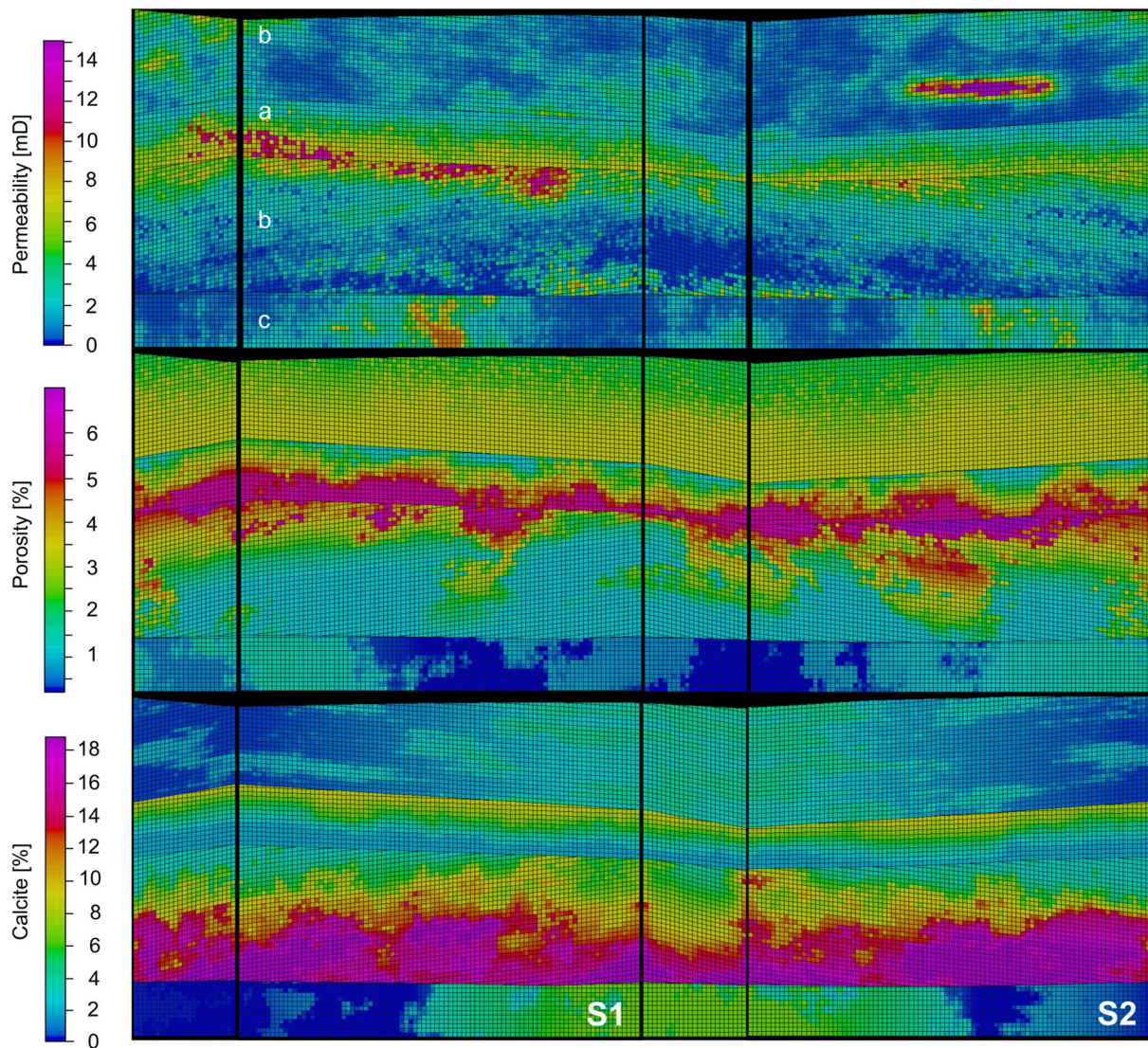


Fig. 11 Warp-around visualization of the block surfaces showing the model results of permeability, porosity, and calcite cement concentration, calculated with a voxel resolution of 5 mm, overall model size = 39 cm (height) × 45 cm (length) × 11.5 cm (depth). The model illustrates the spatial heterogeneity of permeability and explains it by

and permeability are controlled by the amount of calcite cement in this example. This result, and the fact that three independent models that were not created using the relationships between the parameters as a model input, shows that an SGS algorithm can create a highly accurate model reproducing the reservoir characteristics based on the parameter's heterogeneity. The upper cross-bedded section and the fluvial section do not show any correlation between porosity and permeability because the thin sections did not represent the same reservoir conditions as the location of the permeability measurement. This shows that the input data density is critical in the creation of a good model. Even though the permeability and the porosity data did not provide an

porosity and calcite cementation patterns. In particular, the permeability variability of facies sections (a) and lower (b) can be explained by the observed porosity and calcite cementation heterogeneity. The upper (b) section is characterized by low calcite and locally enhanced quartz cement concentrations

effective match in these two sections, the fact that the thin section data does not show a correlation between porosity and the amount of calcite cement suggests a good result. It shows that in those two sections, the reservoir quality is not controlled by the amount of calcite cement, a conclusion that is supported by the petrological investigation of the thin sections and expected by previous results (Fischer et al. 2012).

Furthermore, this shows that a workflow that uses well-defined petrographic data with a focus on diagenetic facies is capable of creating a highly accurate 3D rock property model. In addition, this model can display the cm- to dm-scale reservoir variations and add important insight into how the reservoir was formed by looking at the correlation

between the different input parameters. Finally, this model can provide an indication of where specific levels of reservoir heterogeneity can be expected in a given sedimentary facies.

Conclusions

A portable handheld air permeameter is an efficient tool for enabling fast high-resolution permeability measurements on sample profiles. The resulting data provided insight into the spatial permeability distribution, aiding in the selection of relevant samples for petrographic investigations covering the full range of reservoir properties.

Reservoir quality in the Parchim Formation is controlled by the volume of early poikilitic cement and by the presence of illite/iron oxide grain coatings inhibiting syntaxial K-feldspar and quartz overgrowth. This sub-cm-scale variability highlights the need for high-resolution diagenetic facies mapping and permeability pattern analysis.

Numerical approaches offer the opportunity of providing quantitative and spatial insight into pattern formation of diagenetic features and sedimentary facies. This study shows the promising approach of combining high-resolution diagenetic investigations and 3D modelling using an SGS algorithm. Several sensitivity analyses underscored the reproducibility of a model implementing small-scale reservoir heterogeneities. By implementing plug-scale reservoir quality variations, the application of such models can improve the accuracy of reservoir quality studies on larger scales.

Reactive transport modeling techniques provide insight into the dynamics of fluid-rock interaction. Thus, high-resolution numerical approaches with a focus on pattern formation of diagenetic products and accompanying permeability distribution, as in this study, are applicable for both parametrization and validation of reactive transport models targeting on diagenetic processes.

Acknowledgements We thank H. Lantzsch (U Bremen) for many helpful discussions related to modeling software. We thank Schlumberger for donating the Petrel software to the University of Bremen, making this project possible. We would also like to thank our proofreader. This study has been conducted in the GEO:N joint project ResKin (Reaction kinetics in reservoir rocks—upscaling and modeling), thus being part of the EES topical issue “Sustainable Utilization of Geosystems.” We gratefully acknowledge funding by the German Federal Ministry of Education and Research (BMBF), Grant 03G0871.

Funding Open Access funding enabled and organized by Projekt DEAL.

Open Access This article is licensed under a Creative Commons Attribution 4.0 International License, which permits use, sharing, adaptation, distribution and reproduction in any medium or format, as long as you give appropriate credit to the original author(s) and the source, provide a link to the Creative Commons licence, and indicate if changes

were made. The images or other third party material in this article are included in the article’s Creative Commons licence, unless indicated otherwise in a credit line to the material. If material is not included in the article’s Creative Commons licence and your intended use is not permitted by statutory regulation or exceeds the permitted use, you will need to obtain permission directly from the copyright holder. To view a copy of this licence, visit <http://creativecommons.org/licenses/by/4.0/>.

References

- Ajdkiewicz JM, Lander RH (2010) Sandstone reservoir quality prediction: the state of the art. *AAPG Bull* 94(8):1083–1091
- Bjørlykke K, Jahren J (2012) Open or closed geochemical systems during diagenesis in sedimentary basins: constraints on mass transfer during diagenesis and the prediction of porosity in sandstone and carbonate reservoirs. *AAPG Bull* 96(12):2193–2214
- Brown S, Smith M (2013) A transient-flow syringe air permeameter. *Geophysics* 78(5):D307–D313
- Conford C (1998) Source rocks and hydrocarbons of the North Sea. In: Glennie KW (ed) *Petroleum geology of the North Sea*. Blackwell, Oxford, pp 376–462
- De Boever W, Bultreys T, Derluyn H, Van Hoorebeke L, Cnudde V (2016) Comparison between traditional laboratory tests, permeability measurements and CT-based fluid flow modelling for cultural heritage applications. *Sci Total Environ* 554–555:102–112
- Dolbert C (1998) *Das Oberrotliegend im Flechtinger Höhenzug bei Bebertal, Sachsen Anhalt*. Diplomarbeit Thesis, Christian-Albrechts-Universität, Kiel
- Ellenberg J, Falk F, Grumbt E, Lütznert H, Ludwig AO (1976) Sedimentation des höheren Unterperms der Flechtinger Scholle. *Z Geol Wiss* 4(5):705–737
- Filomena CM, Hornung J, Stollhofen H (2014) Assessing accuracy of gas-driven permeability measurements: a comparative study of diverse Hassler-cell and probe permeameter devices. *Solid Earth* 5(1):1–11
- Fischer C (2013) Sedimentation im Karbon und Rotliegenden des Flechtinger Höhenzuges bei Magdeburg (Sachsen-Anhalt) (Exkursion F am 4. April 2013). *Jahresberichte und Mitteilungen des Oberrheinischen Geologischen Vereins*, pp 107–130
- Fischer C, Gaupp R, Dimke M, Sill O (2007) A 3D high resolution model of bounding surfaces in aeolian-fluvial deposits: an outcrop analogue study from the Permian Rotliegend, Northern Germany. *J Pet Geol* 30(3):257–273
- Fischer C, Dunkl I, von Eynatten H, Wijbrans JR, Gaupp R (2012) Products and timing of diagenetic processes in Upper Rotliegend sandstones from Bebertal (North German Basin, Parchim Formation, Flechtingen High, Germany). *Geol Mag* 149(5):827–840
- Fischer C, Waldmann S, von Eynatten H (2013) Spatial variation in quartz cement type and concentration: an example from the Heidelberg formation (Teufelsmauer outcrops), Upper Cretaceous Subhercynian Basin, Germany. *Sediment Geol* 291:48–61
- Fryberger SG (1993) A review of aeolian bounding surfaces, with examples from the Permian Minnelusa Formation, USA. In: North CP, Prosser DJ (eds) *Characterization of fluvial and aeolian reservoirs*. Geological Society Special Publications: London, pp 167–197
- Fryberger SG, Schenk CJ (1988) Pin stripe lamination—a distinctive feature of modern and ancient eolian sediments. *Sed Geol* 55(1–2):1–15
- Gast R et al (2010) Rotliegend. In: Doornenbal H, Stevenson A (eds) *Petroleum geological atlas of the Southern Permian Basin area*. EAGE Publications, Houten

- Gaupp R (1996) Diagenesis types and their application in diagenesis mapping. *Zentralblatt für Geologie und Paläontologie*, Teil 1, 1994 11/12:1183–1199
- Gaupp R, Okkerman J (2011) Diagenesis and reservoir quality of Rotliegend sandstones in the northern Netherlands—a review. *The Permian Rotliegend of the Netherlands*, vol 98. SEPM special publication, Tulsa, pp 193–226
- Gaupp R, Matter A, Platt J, Ramseyer K, Walzebeck J (1993) Diagenesis and fluid evolution of deeply buried Permian (Rotliegend) gas-reservoirs, Northwest Germany. *AAPG Bull* 77(7):1111–1128
- Gemmer L, Nielsen SB, Bayer U (2003) Late Cretaceous-Cenozoic evolution of the North German Basin—results from 3-D geodynamic modelling. *Tectonophysics* 373(1–4):39–54
- Glennie KW (1986) Development of NW Europe's Southern Permian gas basin, vol 23. Geological Society Special Publications, London, no 1, pp 3–22
- Glennie KW, Mudd GC, Nagtegaal PJC (1978) Depositional environment and diagenesis of Permian Rotliegendes sandstones in Leman Bank and Sole Pit areas of the UK southern North Sea. *J Geol Soc* 135(1):25–34
- Grötsch J, Gaupp R (2011) The Permian Rotliegend of the Netherlands. SEPM (Society for Sedimentary Geology), Tulsa
- Grötsch J et al (2011) The Groningen gas field: fifty years of exploration and gas production from a Permian dryland reservoir. *Permian Rotliegend Neth* 98:11–33
- Hale S, Naab C, Butscher C, Blum P (2019) Method comparison to determine hydraulic apertures of natural fractures. *Rock Mech Rock Eng* 53:1467–1476
- Huysmans M, Peeters L, Moermans G, Dassargues A (2008) Relating small-scale sedimentary structures and permeability in a cross-bedded aquifer. *J Hydrol* 361(1):41–51
- Jones RR et al (2009) Integration of regional to outcrop digital data: 3D visualisation of multi-scale geological models. *Comput Geosci* 35(1):4–18
- Jones FH, Scherer CM, Kuchle J (2016) Facies architecture and stratigraphic evolution of aeolian dune and interdune deposits, Permian Caldeirão Member (Santa Brígida Formation), Brazil. *Sediment Geol* 337:133–150
- Kimple D, Peterson EW, Malone DH (2015) Stratigraphy and Porosity Modeling of South-Central Illinois (USA) chester (upper mississippian) series sandstones using petrel. *World J Environ Eng* 3(3):82–86
- Kleditzsch O, Kurze M (1993) Ergebnisse petrographischer Untersuchungen an Sandsteinen des tieferen Oberrotliegenden im Raum Altmark/Westmecklenburg. *Geologisches Jahrbuch A* 131:141–178
- Kulke H, Gast R, Helmuth H, Lütznert H (1993) Harz Area, Germany: typical Rotliegend and Zechstein reservoirs in the Southern Permian Basin (Central Europe). In: Houwer JM, Pilaar WF, Graaff-Trouwborst T (eds) AAPG international conference & exhibition, The Hague, October 1993. PGK, pp 87
- McBride EF, Land L, Mack L (1987) Diagenesis of eolian and fluvial feldspathic sandstones, Norphlet Formation (Upper Jurassic), Rankin County, Mississippi, and Mobile County, Alabama. *AAPG Bull* 71(9):1019–1034
- Molenaar N, Felder M, Bär K, Götz AE (2015) What classic greywacke (litharenite) can reveal about feldspar diagenesis: an example from Permian Rotliegend sandstone in Hessen, Germany. *Sed Geol* 326:79–93
- Molz FJ III, Dinwiddie CL, Wilson JL (2003) A physical basis for calculating instrument spatial weighting functions in homogeneous systems. *Water Resour Res* 39(4):1096. <https://doi.org/10.1029/2001WR001220>
- Morad S, Al-Ramadan K, Ketzer JM, De Ros LF (2010) The impact of diagenesis on the heterogeneity of sandstone reservoirs: a review of the role of depositional facies and sequence stratigraphy. *AAPG Bull* 94(8):1267–1309
- Mountney NP, Jagger A (2004) Stratigraphic evolution of an aeolian erg margin system: the Permian Cedar Mesa Sandstone, SE Utah, USA. *Sedimentology* 51(4):713–743
- Mountney N, Howell J, Flint S, Jerram D (1998) Aeolian and alluvial deposition within the Mesozoic Etjo Sandstone Formation, northwest Namibia. *J Afr Earth Sci* 27(2):175–192
- Plein E (1993) Bemerkungen zum Ablauf der paläogeographischen Entwicklung im Stefan und Rotliegend des Norddeutschen Beckens. *Geol Jahrb* 1993(131):99–116
- Poszytek A (2013) Reservoir properties of the Upper Rotliegend and the Weissliegend sandstones in the Zielona Góra Basin (western Poland). *Geol Q* 58(1):193–206. <https://doi.org/10.7306/gq.1140>
- Pyrz MJ, Deutsch CV (2014) Geostatistical reservoir modeling. Oxford University Press, Oxford
- Rogiers B et al (2014a) The usefulness of outcrop analogue air permeameter measurements for analyzing aquifer heterogeneity: quantifying outcrop hydraulic conductivity and its spatial variability. *Hydrol Process* 28(20):5176–5188
- Rogiers B et al (2014b) High-resolution saturated hydraulic conductivity logging of borehole cores using air permeability measurements. *Hydrogeol J* 22(6):1345–1358
- Scherer CMS, Lavina ELC (2005) Sedimentary cycles and facies architecture of aeolian-fluvial strata of the Upper Jurassic Guará Formation, Southern Brazil. *Sedimentology* 52(6):1323–1341
- Schöner R, Gaupp R (2005) Contrasting red bed diagenesis: the southern and northern margin of the Central European Basin. *Int J Earth Sci* 94(5–6):897–916
- Schreiber A (1960) Das Rotliegende des Flechtinger Höhenzuges. *Freib Forsch C* 82:1–132
- Taylor TR et al (2010) Sandstone diagenesis and reservoir quality prediction: models, myths, and reality. *AAPG Bull* 94(8):1093–1132
- Taylor TR, Kittridge MG, Winefield P, Bryndzia LT, Bonnell LM (2015) Reservoir quality and rock properties modeling—Triassic and Jurassic sandstones, greater Shearwater area, UK Central North Sea. *Mar Pet Geol* 65:1–21
- Wong, T.E., Batjes, D.A., de Jager, J., 2007. *Geology of the Netherlands*. Editat—the Publishing House of the Royal
- Worden RH, Matray JM (1998) Carbonate cement in the Triassic Chaunoy Formation of the Paris Basin: distribution and effect on flow properties. In: Morad S (ed) Carbonate cementation in sandstones: distribution patterns and geochemical evolution. International Association of Sedimentologists Special Publication 26, pp 163–177. ISBN: 978-0-632-04777-2
- Worden RH et al (2018) Petroleum reservoir quality prediction: overview and contrasting approaches from sandstone and carbonate communities. *Geol Soc Lond Spec Publ* 435(1):1–31

Publisher's Note Springer Nature remains neutral with regard to jurisdictional claims in published maps and institutional affiliations.